Aalto University

Hannonen, Antti; Saastamoinen, Kimmo; Leppanen, Lasse-Petteri; Koivurova, Matias; Shevchenko, Andriy; Friberg, Ari T.; Setala, Tero

Geometric phase in beating of light waves

PAPER • OPEN ACCESS

Geometric phase in beating of light waves

View the article online for updates and enhancements.

New Journal of Physics

The open access journal at the forefront of physics

Deutsche Physikalische Gesellschaft **DPG**

IOP Institute of Physics

Published in partnership with: Deutsche Physikalische Gesellschaft and the Institute of Physics

CrossMark

PAPER

Geometric phase in beating of light waves

Antti Hannonen[1], Kimmo Saastamoinen[1], Lasse-Petteri Leppänen[1,3], Matias Koivurova[1], **Andriy Shevchenko[2], Ari T Friberg[1]** and **Tero Setälä[1]**

1. Institute of Photonics, University of Eastern Finland, PO Box 111, FI-80101 Joensuu, Finland
2. Department of Applied Physics, Aalto University, PO Box 13500, FI-00076 Aalto, Finland
3. Current address: Microsoft, Keilalahdentie 2-4, FI-02150, Espoo, Finland.

E-mail: antti.hannonen@uef.fi

Abstract

Beating is a simple physical phenomenon known for long in the context of sound waves but remained surprisingly unexplored for light waves. When two monochromatic optical beams of different frequencies and states of polarization interfere, the polarization state of the superposition field exhibits temporal periodic variation—polarization beating. In this work, we reveal a foundational and elegant phase structure underlying such polarization beating. We show that the phase difference over a single beating period decomposes into the Pancharatnam–Berry geometric phase and a dynamical phase of which the former depends exclusively on the intensities and polarization states of the interfering beams whereas the sum of the phases is determined solely by the beam frequencies. Varying the intensity and polarization characteristics of the beams, the relative contributions of the geometric and dynamical phases can be adjusted. The geometric phase inherent in polarization beating is governed by a compact expression containing only the Stokes parameters of the interfering waves and can alternatively be obtained from the individual beam intensities and the amplitude of the intensity beats. We demonstrate both approaches experimentally by using an interferometer with a fast detector and a specific polarimetric arrangement. Polarization beating has a unique character that the geometric and dynamical phases are entangled, i.e. variation in one unavoidably leads to a change in the other. Our work expands geometric phases into a new domain and offers important novel insight into the role of polarization in interference of electromagnetic waves.

1. Introduction

Beating is a temporal interference phenomenon in which waves of different frequencies form a superposition with periodically varying characteristics. The effect is often encountered in the field of acoustics but also exists in the context of light waves [1], e.g. in laser mode locking [2], heterodyne detection [3], frequency stabilization [4, 5], and optical velocimetry [6]. In addition, electro-optic and acousto-optic modulators create frequency shifts enabling beating of light waves observable with modern detectors [7, 8]. In electromagnetic optics, however, not only does the intensity experience beating but also (or only) the polarization state may vary periodically giving rise to the effect of polarization beating [9, 10].

The Pancharatnam–Berry geometric phase emerges when the polarization state of light traces out a closed in-phase loop on the Poincaré sphere [11–13]. The phase is caused by the geometry of the curved polarization space and is equal to half the solid angle subtended by the polarization trajectory. This remarkable result, first formulated in 1956 by Pancharatnam [14], has been the subject of extensive research [11, 15] after Berry discovered a topological phase that appears in dynamical quantum systems [16] and demonstrated its similarity with Pancharatnam's optical phase [17, 18]. However, earlier studies in optics have focused on the geometric phase in the spatial domain when light traverses a sequence of optical elements, or when photons are made to complete a series of changes in their propagation directions (spin-redirection phase) [19–24]. Very recently, the geometric phase was assessed in the context of surface plasmon waves [25] and Young's double-pinhole

experiment, where interfering electromagnetic fields emanating from the apertures form a spatially periodic polarization pattern [26]. The notion of Pancharatnam–Berry phase also appears extensively in connection of the so-called geometric phase metasurfaces [27–29].

In this paper, we consider the Pancharatnam–Berry phase in the time domain and in a completely new context, namely polarization beating of two monochromatic electromagnetic beams of different frequencies. During a single beating period, the normalized Poincaré vector is shown to traverse a closed circular loop on the Poincaré sphere leading to a geometric phase which is in a simple manner connected to the Stokes parameters of the interfering beams. We further show that the phase can alternatively be found by considering the individual beam intensities and the amplitude of the intensity beats. Both methods are demonstrated experimentally. The geometric phase in polarization beating depends only on the intensities and polarization states of the interfering beams, while the sum of the geometric and dynamical phase is solely determined by the beam frequencies. The beating of vector light waves therefore features a fundamental entangled character of the geometric and dynamical phases. This novel property allows one to adjust either of the two phases via the intensities and the polarization states of the waves, which may have practical consequences in electromagnetic interferometry and other phase-sensitive measurement techniques. In general, our work reveals a new, unexpected phase structure pertaining to the temporal interference of vector light beams.

2. Temporal electromagnetic interference

We begin by examining the temporal interference of two monochromatic (deterministic) electromagnetic beams of different frequencies, taken to propagate along the *z* axis. The fields can be written as

$$\mathbf{E}_m(t) = \mathbf{E}_m \exp(-i\omega_m t), \quad m \in \{1, 2\}, \tag{1}$$

where ω_m is an angular frequency and t refers to time. The vector $\mathbf{E}_m = [E_{m,x}, E_{m,y}]^{\mathrm{T}}$ is the electric field amplitude composed of the transverse x and y components $E_{m,x}, E_{m,y}$ and T denotes the transpose. Above, the explicit dependency on the spatial coordinate was dropped as we consider the fields at a fixed point. The superposition of the two monochromatic beams can be expressed in the form

$$\mathbf{E}(t) = \mathbf{E}_1(t) + \mathbf{E}_2(t) = \exp(-i\omega t) \begin{bmatrix} E_{1,x} \exp(i\Delta\omega t/2) + E_{2,x} \exp(-i\Delta\omega t/2) \\ E_{1,y} \exp(i\Delta\omega t/2) + E_{2,y} \exp(-i\Delta\omega t/2) \end{bmatrix}, \tag{2}$$

where $\Delta\omega = \omega_2 - \omega_1$ (we assume $\omega_2 > \omega_1$) and $\omega = (\omega_1 + \omega_2)/2$ are the frequency difference and the average frequency, respectively.

The traditional (instantaneous) Stokes parameters of the superposition are given in terms of the components of $\mathbf{E}(t)$ as

$$S_0(t) = E_x^*(t)E_x(t) + E_y^*(t)E_y(t), \tag{3a}$$

$$S_1(t) = E_x^*(t)E_x(t) - E_y^*(t)E_y(t), \tag{3b}$$

$$S_2(t) = E_x^*(t)E_y(t) + E_y^*(t)E_x(t), \tag{3c}$$

$$S_3(t) = i[E_y^*(t)E_x(t) - E_x^*(t)E_y(t)], \tag{3d}$$

where the asterisk denotes the complex conjugate. The first parameter, $S_0(t)$, is the instantaneous intensity of the field, while the other three, $S_1(t)$, $S_2(t)$, and $S_3(t)$, characterize its time-varying polarization state [30, 31]. Substituting from equation (2) into equations (3a)–(3d), the Stokes parameters of the total field become

$$S_n(t) = S_n' + S_n'' + 2\Re[\mathcal{S}_n \exp(-i\Delta\omega t)], \quad n \in \{0, \ldots, 3\}, \tag{4}$$

where $\Re$ stands for the real part. The terms S_n' and S_n'' denote the Stokes parameters of the individual beams $\mathbf{E}_1(t)$ and $\mathbf{E}_2(t)$, respectively, whereas the (complex) quantities $\mathcal{S}_n$ are

$$\mathcal{S}_0 = E_{1,x}^* E_{2,x} + E_{1,y}^* E_{2,y}, \tag{5a}$$

$$\mathcal{S}_1 = E_{1,x}^* E_{2,x} - E_{1,y}^* E_{2,y}, \tag{5b}$$

$$\mathcal{S}_2 = E_{1,x}^* E_{2,y} + E_{1,y}^* E_{2,x}, \tag{5c}$$

$$\mathcal{S}_3 = i(E_{1,y}^* E_{2,x} - E_{1,x}^* E_{2,y}). \tag{5d}$$

The intensity-normalized versions of these quantities are of the form

$$\gamma_n = \frac{\mathcal{S}_n}{\sqrt{S_0' S_0''}}, \quad n \in \{0, \ldots, 3\}. \tag{6}$$

The quantities in equations (5a)–(5d) are analogous to the two-point Stokes parameters introduced for random light beams and discussed, e.g. in [32, 33] but evaluated here between two deterministic fields.

Inserting $\mathcal{S}_n$ from equation (6) into (4) leads to

$$S_n(\alpha) = S_n' + S_n'' + 2\sqrt{S_0' S_0''}\,|\gamma_n|\cos\left[\arg(\gamma_n) - \alpha\right], \quad n \in \{0, \ldots, 3\}, \tag{7}$$

where $\arg(z)$ denotes the argument (phase) of a complex number z and we introduced $\alpha = \Delta\omega t$. Notice that S_n', S_n'', and γ_n are independent of time for all $n \in \{0, \ldots, 3\}$ and the only time dependence is in the α term. The above result is a temporal electromagnetic interference law for two monochromatic light beams of different frequencies describing how the interference modulates the intensity and the polarization state. In particular, the last term in equation (7) indicates that the modulation is sinusoidal at angular frequency $\Delta\omega$ and temporal period $T = 2\pi/\Delta\omega$. When the frequencies are identical, the modulation vanishes. The modulation may occur either for intensity or polarization state or for both simultaneously, depending on the polarization states of the constituent beams as expressed by γ_n, $n \in \{0, \ldots, 3\}$, whose magnitudes specify the modulation amplitudes. We refer to this periodic temporal variation as beating of electromagnetic waves or, especially, polarization beating if the effect takes place for the polarization state. Notice that the beating of $S_1(\alpha)$, $S_2(\alpha)$, and $S_3(\alpha)$ does not necessarily indicate a temporal variation of the polarization state. In particular, if the polarization states of the interfering beams are identical, some or all of the polarization-state Stokes parameters may vary periodically with time but the related polarization state remains invariant. More precisely, the intensity-normalized Stokes parameters, $s_n = S_n(\alpha)/S_0(\alpha)$, with $n \in \{1, 2, 3\}$, are constant and only the intensity exhibits beating. We remark that electromagnetic interference laws analogous to equation (7), but in the context of random light, have been considered earlier [9, 10, 34, 35].

3. Pancharatnam–Berry phase in temporal interference

Polarization beating of two monochromatic light waves leads to the generation of Pancharatnam–Berry geometric phase between the total fields separated by the time period T. In this section, we derive an expression for this phase in terms of the polarization-state and intensity information of the interfering beams. We also show that, alternatively, the phase is obtained by measuring the individual beam intensities and the amplitude of the intensity beating.

3.1. Polarization path analysis
Equation (7) implies directly that the polarization state of the superposition field is a periodic function of α. Accordingly, the Poincaré unit vector [30, 31]

$$\hat{\mathbf{P}}(\alpha) = \frac{\mathbf{P}(\alpha)}{S_0(\alpha)} = \frac{\hat{\mathbf{s}}_1 S_1(\alpha) + \hat{\mathbf{s}}_2 S_2(\alpha) + \hat{\mathbf{s}}_3 S_3(\alpha)}{S_0(\alpha)}, \tag{8}$$

which specifies the instantaneous polarization state, is also periodic. Here $\mathbf{P}(\alpha)$ is the unnormalized Poincaré vector and $\hat{\mathbf{s}}_n$, $n \in \{1, 2, 3\}$, are the orthogonal unit vectors in the polarization space defined by the Poincaré sphere depicted in figure 1. Making use of equations (7) and (8), the unit vector $\hat{\mathbf{P}}(\alpha)$ can be expressed as

$$\hat{\mathbf{P}}(\alpha) = \frac{\mathbf{P}' + \mathbf{P}'' + 2\sqrt{S_0' S_0''}\,[\Re(\boldsymbol{\gamma})\cos\alpha + \Im(\boldsymbol{\gamma})\sin\alpha]}{S_0' + S_0'' + 2\sqrt{S_0' S_0''}\,[\Re(\gamma_0)\cos\alpha + \Im(\gamma_0)\sin\alpha]}, \tag{9}$$

where $\mathbf{P}'$ and $\mathbf{P}''$ are the Poincaré vectors of the individual beams, $\boldsymbol{\gamma} = \hat{\mathbf{s}}_1\gamma_1 + \hat{\mathbf{s}}_2\gamma_2 + \hat{\mathbf{s}}_3\gamma_3$, and $\Im$ denotes the imaginary part. The above equation gives an explicit expression for the periodic path that the Poincaré unit vector traces on the Poincaré sphere when two monochromatic electromagnetic beams interfere. If the denominator of equation (9) is zero at some point, $\hat{\mathbf{P}}(\alpha)$ is undefined. This corresponds to a circumstance in which the interfering beams are in the same state of polarization and no polarization beating takes place. This situation is excluded from the following analysis.

The periodic in-phase change in the polarization state gives rise to a Pancharatnam–Berry phase whose magnitude is equal to half the solid angle enclosed by the path of $\hat{\mathbf{P}}(\alpha)$ on the surface of the Poincaré sphere [12, 13]. Thus the shape of the polarization trajectory given in equation (9) determines the phase generated over a single beating period. In order to analyze the path of $\hat{\mathbf{P}}(\alpha)$ in more detail, it is necessary to introduce certain relationships between the quantities presented above. First, it follows at once from the definitions that

$$S_0' = |\mathbf{P}'|, \quad S_0'' = |\mathbf{P}''|, \tag{10a}$$

$$|\gamma_0|^2 + |\boldsymbol{\gamma}|^2 = 2. \tag{10b}$$

Second, use of equations (9)–(10b), the fact that $|\hat{\mathbf{P}}(\alpha)| = 1$, and the uniqueness of the Fourier-series representation yield the following four relations

$$\hat{\mathbf{P}}' \cdot \hat{\mathbf{P}}'' = 2|\gamma_0|^2 - 1, \tag{11a}$$

$$\boldsymbol{\gamma} \cdot (\mathbf{P}' + \mathbf{P}'') = \gamma_0(S_0' + S_0''), \tag{11b}$$
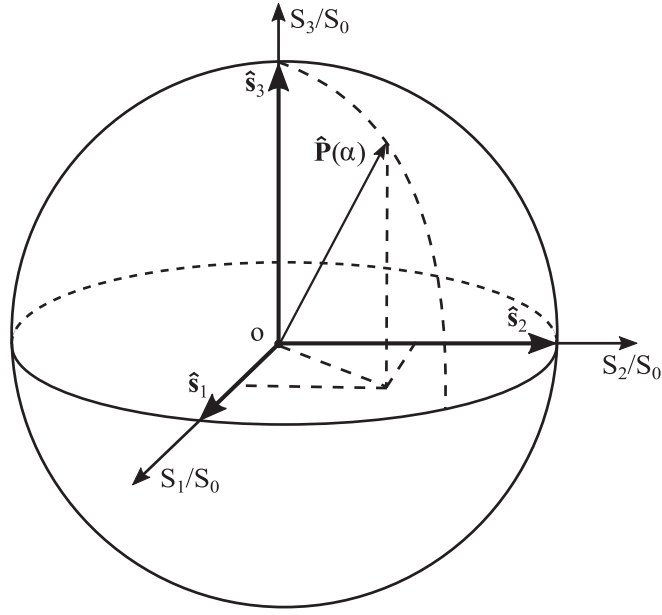
Figure 1. Poincaré unit sphere in the polarization space formed by the three Stokes parameters S_1, S_2, and S_3. The sphere is centered at the origin and the basis vectors $\hat{s}_1$, $\hat{s}_2$, and $\hat{s}_3$ are orthonormal. Each point on the sphere uniquely specifies a polarization state as represented by the normalized Poincaré vector $\hat{\mathbf{P}}(\alpha)$. Linear and spherical polarization states are located on the equator and the poles, respectively, while elliptical polarization states are distributed between them.
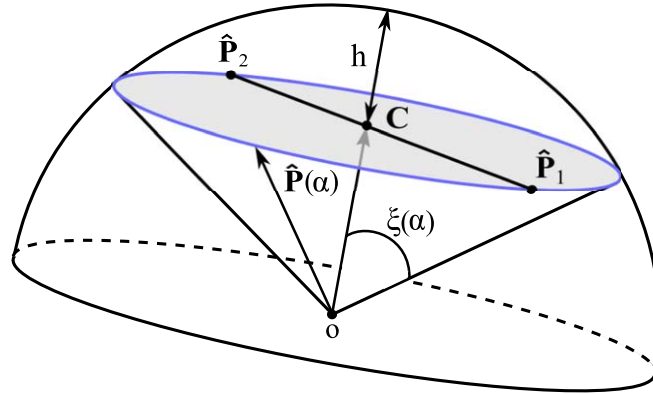

Figure 2. Notation used in deriving the Pancharatnam–Berry phase associated with polarization beating. The blue line corresponds to the circular path of $\hat{\mathbf{P}}(\alpha)$, while $\mathbf{C} = (\hat{\mathbf{P}}_1 + \hat{\mathbf{P}}_2)/2$ denotes the center point of the circle. The angle between the two vectors is $\xi(\alpha)$ and h is the height of the spherical cap.

$$\gamma^2 = \gamma_0^2, \tag{11c}$$

$$\Re(\gamma) \cdot \Im(\gamma) = \Re(\gamma_0)\Im(\gamma_0), \tag{11d}$$

where the terms $\hat{\mathbf{P}}'$ and $\hat{\mathbf{P}}''$ correspond to the normalized Poincaré vectors of the constituent beams.

In the following we show that $\hat{\mathbf{P}}(\alpha)$ forms a circle on the Poincaré sphere as a function of α. Such a property can be proven by finding a constant vector $\mathbf{C}$ which satisfies $\mathbf{C} \cdot \hat{\mathbf{P}}(\alpha) = |\mathbf{C}| \cos[\xi(\alpha)] = $ constant, where $\xi(\alpha)$ is the angle between $\mathbf{C}$ and $\hat{\mathbf{P}}(\alpha)$. As illustrated in figure 2, geometrically this requires that $\xi(\alpha)$ remains unchanged as α varies. As will be shown, a vector that satisfies the above condition is

$$\mathbf{C} = \frac{1}{2}(\hat{\mathbf{P}}_1 + \hat{\mathbf{P}}_2), \tag{12}$$

where $\hat{\mathbf{P}}_1 = \hat{\mathbf{P}}[\arg(\gamma_0)]$, $\hat{\mathbf{P}}_2 = \hat{\mathbf{P}}[\arg(\gamma_0) \pm \pi]$, and the sign is chosen such that the argument of $\hat{\mathbf{P}}$ remains within the half-open interval $[0, 2\pi)$. Thus, $\mathbf{C}$ is located halfway between the points $\hat{\mathbf{P}}_1$ and $\hat{\mathbf{P}}_2$. On substituting equation (9) into (12) and employing equations (10a) and (11a), we may express $\mathbf{C}$ in the form

$$\mathbf{C} = \frac{(\mathbf{P}' + \mathbf{P}'')(S_0' + S_n'') - 4S_0'S_0'' \left[\mathfrak{R}(\gamma)\mathfrak{R}(\gamma_0) + \mathfrak{I}(\gamma)\mathfrak{I}(\gamma_0)\right]}{|\mathbf{P}' - \mathbf{P}''|^2}. \tag{13}$$

To evaluate the dot product, we make use of equations (13) and (9)–(11*c*). After straightforward steps, we find that

$$\mathbf{C} \cdot \hat{\mathbf{P}}(\alpha) = \frac{(S_0' - S_0'')^2}{|\mathbf{P}' - \mathbf{P}''|^2}, \tag{14}$$

which is indeed constant. Hence, it is clear that the points of $\hat{\mathbf{P}}(\alpha)$ are located on a circle, at least when $\mathbf{C} \neq 0$ and $\mathbf{P}' \neq \mathbf{P}''$ hold. In view of equation (12), $\mathbf{C}$ is the center point of the circle and $\hat{\mathbf{P}}_1$ and $\hat{\mathbf{P}}_2$ form a pair of antipodal points. In the case of $\mathbf{C} = 0$, it is possible to show that the path traced by the Poincaré unit vector becomes a great circle (as seen also from figure 2 in the limit $\mathbf{C} \to 0$) and equation (14) remains valid. In the situation when $\mathbf{P}' = \mathbf{P}''$, the polarization states of the interfering beams are identical and no polarization beating takes place; the case was already excluded.

So far we have shown that the points of $\hat{\mathbf{P}}(\alpha)$ are located on a circle on the Poincaré sphere. To prove that a closed path is obtained we first notice that according to equation (8) the vector $\hat{\mathbf{P}}(\alpha)$ is continuous. Additionally, we should show that all the values of α are mapped to different points, i.e. that $\hat{\mathbf{P}}(\alpha)$ is a bijective function from the set $[0, 2\pi)$ to the points of the circle. To prove such a property, we must demonstrate that the equality $\hat{\mathbf{P}}(\alpha_1) = \hat{\mathbf{P}}(\alpha_2)$ holds if, and only if, $\alpha_1 = \alpha_2$. On assuming that $\hat{\mathbf{P}}(\alpha_1) = \hat{\mathbf{P}}(\alpha_2)$ it at once follows from $|\hat{\mathbf{P}}(\alpha)| = 1$ that $\hat{\mathbf{P}}(\alpha_1) \cdot \hat{\mathbf{P}}(\alpha_2) = 1$. Inserting from equation (9) and invoking equations (10*a*)–(11*d*), we find the following relationship

$$(|\gamma_0|^2 - 1) + \cos(\alpha_1 - \alpha_2)(1 - |\gamma_0|^2) = 0. \tag{15}$$

This expression is satisfied if $|\gamma_0| = 1$ or $\cos(\alpha_1 - \alpha_2) = 1$. According to equation (11*a*), the former condition leads to the excluded case of identical polarization states of the beams. Consequently, the latter solution must hold, requiring that $\alpha_1 = \alpha_2$. As $\hat{\mathbf{P}}(\alpha)$ is continuous we thus find that every point of the circle is mapped to a unique value of α.

According to Pancharatnam's connection [13, 17], two arbitrary fields $\mathbf{E}_1$ and $\mathbf{E}_2$ are in phase when their superposition has the maximum possible intensity. This corresponds to a situation where $\mathfrak{R}(\mathbf{E}_1^* \cdot \mathbf{E}_2) > 0$ and $\mathfrak{I}(\mathbf{E}_1^* \cdot \mathbf{E}_2) = 0$ or, equivalently, $\arg(\mathbf{E}_1^* \cdot \mathbf{E}_2) = 0$. In the present case, at any point on the polarization path we may write

$$\lim_{\Delta\alpha \to 0} [\mathbf{E}^*(\alpha) \cdot \mathbf{E}(\alpha + \Delta\alpha)] = \mathbf{E}^*(\alpha) \cdot \mathbf{E}(\alpha) = S_0(\alpha) > 0, \tag{16}$$

implying that $\lim_{\Delta\alpha \to 0} \arg[\mathbf{E}^*(\alpha) \cdot \mathbf{E}(\alpha + \Delta\alpha)] = 0$. Hence, when the Poincaré unit vector $\hat{\mathbf{P}}(\alpha)$ traverses from one point to another, the electric field $\mathbf{E}(\alpha)$ obeys Pancharatnam's connection and experiences in-phase evolution.

Now it is possible to derive an expression for the Pancharatnam–Berry geometric phase. By taking the squared magnitude of $\mathbf{C}$ in equation (13) and employing equations (10*a*)–(11*d*), the length of vector $\mathbf{C}$ turns out to be

$$|\mathbf{C}| = \frac{|S_0' - S_0''|}{|\mathbf{P}' - \mathbf{P}''|}. \tag{17}$$

The surface area of a spherical dome is $A = 2\pi r h$, where r is the radius of the sphere and h is the height of the dome (see figure 2). Since we are considering a unit sphere, $r = 1$, $h = 1 - |\mathbf{C}|$, and the solid angle Ω subtended by $\hat{\mathbf{P}}(\alpha)$ is simply equal to the surface area of the cap. The geometric phase, $|\phi_{\mathrm{PB}}| = \Omega/2$, related to the in-phase polarization evolution over a single beating period therefore takes the form

$$|\phi_{\mathrm{PB}}| = \pi - \pi \frac{|S_0' - S_0''|}{|\mathbf{P}' - \mathbf{P}''|}. \tag{18}$$

In accordance with the definition of Pancharatnam, the phase is positive when $\hat{\mathbf{P}}(\alpha)$ traces the path counterclockwise and negative otherwise [14]. The magnitude of the geometric phase is determined by the intensities and the polarization states of the two beams. For example, we see from equation (18) that if the intensities of the two beams are equal, then independently of the polarization states, $|\phi_{\mathrm{PB}}| = \pi$ and the polarization path is a great circle. In general, when the intensities are unequal, the magnitude of ϕ_{PB} can take on any value between 0 and π.

3.2. Phase evaluation

Next we show that an alternative way to obtain the Pancharatnam–Berry phase over a single beating period is in terms of the intensities of the interfering beams and $|\gamma_0|$ specifying the amplitude of the intensity beating. The beating period from t_0 to $t_0 + T$ is divided into N small intervals with N being a large integer so that the fields $\mathbf{E}(t_n)$, $t_n = t_0 + nT/N$ with $n \in \{0, \ldots, N\}$, undergo a polarization change with $\mathbf{E}(t_0)$ and $\mathbf{E}(t_N)$ having identical

polarization states. The total phase difference between $\mathbf{E}(t_0)$ and $\mathbf{E}(t_N)$ is given by $\arg[\mathbf{E}^*(t_N) \cdot \mathbf{E}(t_0)]$ [13, 14]. In general, the phase difference consists of two parts: one is a dynamical phase, ϕ_{dyn}, whereas the other is the Pancharatnam–Berry geometric phase, ϕ_{PB}. From this point of view, it is possible to evaluate ϕ_{PB} by determining how the phase of the electric field is acquired from the incremental parts $\arg[\mathbf{E}^*(t_n) \cdot \mathbf{E}(t_{n-1})]$.

We begin by writing the electric fields as $\mathbf{E}(t_n) = \exp(-i\psi_n)\mathbf{E}'(t_n)$, where ψ_n are phases chosen such that $\mathbf{E}'(t_n)$ obeys Pancharatnam's connection [13, 17], i.e. $\arg[\mathbf{E}'^*(t_n) \cdot \mathbf{E}'(t_{n-1})] = 0$ for all $n \in \{1, \ldots, N\}$. Consequently, the geometric phase can be expressed as

$$\phi_{\mathrm{PB}} = \arg[\mathbf{E}^*(t_N) \cdot \mathbf{E}(t_0)] - \phi_{\mathrm{dyn}}, \tag{19}$$

where

$$\phi_{\mathrm{dyn}} = \sum_{n=1}^{N} \arg[\mathbf{E}^*(t_n) \cdot \mathbf{E}(t_{n-1})] = \psi_N - \psi_0. \tag{20}$$

Making use of equation (2) and the fact that the beating period is $T = 2\pi/\Delta\omega$ and hence $t_n = t_0 + 2\pi n/\Delta\omega N$, with $n \in \{0, \ldots, N\}$, we obtain the total phase as

$$\arg[\mathbf{E}^*(t_N) \cdot \mathbf{E}(t_0)] = \omega(t_N - t_0) \pm \pi, \tag{21}$$

where $t_N - t_0 = T$ and $\pm\pi = \arg(-1)$. Analogously, after some algebra we find that

$$\arg\left[\mathbf{E}^*(t_n) \cdot \mathbf{E}(t_{n-1})\right] = \omega(t_n - t_{n-1}) + \arg\left\{ S_0' \exp\left(\frac{-i\pi}{N}\right) + S_0'' \exp\left(\frac{i\pi}{N}\right) \right.$$
$$\left. + 2\sqrt{S_0'S_0''}\,|\gamma_0|\cos\left[\arg(\gamma_0) - \Delta\omega t_0 - \frac{2\pi n}{N} + \frac{\pi}{N}\right]\right\}. \tag{22}$$

On substituting equations (21) and (22) into (19) and (20), respectively, the Pancharatnam–Berry geometric phase incurred over one beating period can be expressed as

$$\phi_{\mathrm{PB}} = \pm\pi - \sum_{n=1}^{N} \arg\left\{ S_0' \exp\left(\frac{-i\pi}{N}\right) + S_0'' \exp\left(\frac{i\pi}{N}\right) \right.$$
$$\left. + 2\sqrt{S_0'S_0''}\,|\gamma_0|\cos\left[\arg(\gamma_0) - \Delta\omega t_0 - \frac{2\pi n}{N} + \frac{\pi}{N}\right]\right\}, \tag{23}$$

where the sign of π is chosen to conform to the restriction $|\phi_{\mathrm{PB}}| \leqslant \pi$. Because the sum is over the whole beating period, all terms inside the cosine function that are independent of n can be omitted. When the summation is performed numerically for large N, the geometric phase obtained is seen to be fully consistent with equation (18). The parameter γ_0 in the above equation is directly related to the amplitude of the intensity beating. According to equation (7), with $n = 0$, we find that

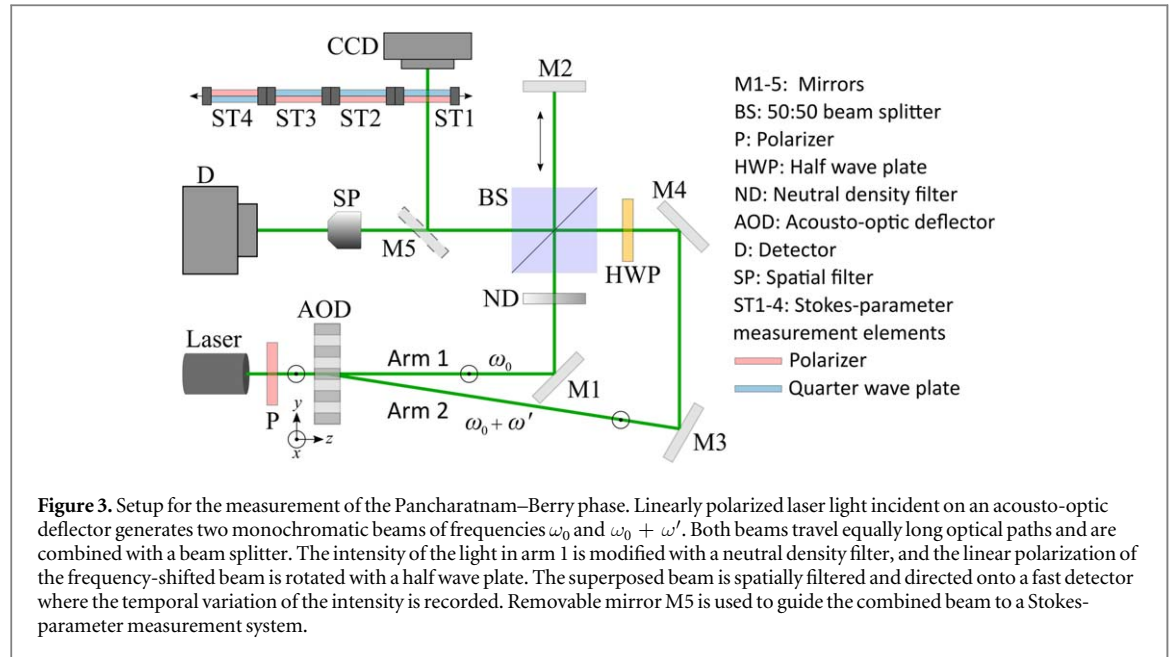$$|\gamma_0| \cos[\arg(\gamma_0) - \alpha(t)] = \frac{S_0(t) - (S_0' + S_0'')}{2\sqrt{S_0'S_0''}}. \tag{24}$$

The geometric phase can thus be extracted from equation (23) by measuring S_0' and S_0'' and determining $|\gamma_0|$ from the temporal intensity modulation via equation (24).

Equations (21) and (23) (or (18)) show that all information on the length of the beating period is in the dynamical phase. We also find the characteristic feature of the geometric phase inherent in polarization beating. More precisely, as evidenced by equation (18) the Pancharatnam–Berry phase is determined exclusively by the intensities and polarization states of the interfering beams while, according to equation (21), the sum of the geometric and dynamical phases depends on the wave frequencies only. Hence, a change in the geometric phase necessarily leads to an alteration of the dynamical phase. As far as we know, such an entanglement of geometric and dynamical phases has not been reported in other contexts.

4. Experiment

In this section, we consider the measurement of the Pancharatnam–Berry phase in polarization beating by utilizing the interferometer illustrated in figure 3. A monochromatic, x-polarized beam (achieved by polarizer P) from a diode-pumped solid state laser (wavelength 532 nm) is directed to an acousto-optic deflector (AOD, IntraAction AOD-150), set to operate at 100 MHz. Along with a beam of the original frequency ω_0 in arm 1, the deflector creates a beam of a shifted frequency $\omega_0 + \omega'$ in arm 2. In order to obtain the maximum diffraction efficiency for the frequency-shifted field, the input-beam incidence on the AOD is at the Bragg angle. The polarization state of the beam in arm 2 may be rotated with a half wave plate (HWP), while the intensity of the beam in arm 1 can be varied with an adjustable neutral density filter (ND). The optical path lengths traversed by

Figure 3. Setup for the measurement of the Pancharatnam–Berry phase. Linearly polarized laser light incident on an acousto-optic deflector generates two monochromatic beams of frequencies ω_0 and $\omega_0 + \omega'$. Both beams travel equally long optical paths and are combined with a beam splitter. The intensity of the light in arm 1 is modified with a neutral density filter, and the linear polarization of the frequency-shifted beam is rotated with a half wave plate. The superposed beam is spatially filtered and directed onto a fast detector where the temporal variation of the intensity is recorded. Removable mirror M5 is used to guide the combined beam to a Stokes-parameter measurement system.

both beams are set equal with a movable mirror M2. This is necessary in order to observe the beating effect at the detector since the AOD induces significant randomness to the frequency-shifted beam, reducing the time interval over which the two beams correlate. However, by considering equal-time interference, the effect of reduced temporal coherence is not relevant and the deterministic-field formalism of the previous section can be employed. Both beams are combined with a nonpolarizing 50:50 beam splitter and directed towards two different detection systems selectable with a removable mirror M5.

In the first measurement system, the beams enter a spatial filtering system (SP) after which they are directed (with lenses) to a high-speed optical detector (D, Newport 818-BB-21) attached to an oscilloscope which records the intensity beating. The spatial filtering is necessary since, in addition to reduced temporal coherence, the AOD decreases the transverse spatial coherence as well. Consequently, the intensity beats at different positions on the detector would not be in phase and the temporal intensity modulation could not be accurately measured.

The second measurement system is used to determine the Stokes parameters using four polarization elements (ST1-ST4) and a CCD camera. The elements consist of combinations of polarizers and quarter wave plates. The polarizer orientations with respect to the polarization direction of the input beam (x axis) are set to $\theta_P = (0°, +90°, +45°, +45°)$, while the quarter wave plate fast-axis angles are $\theta_{QWP} = (+45°, -45°, +90°, +90°)$. The element ST4 is flipped and the beams hit the quarter wave plate first. While the orientations of the wave plates in the other three elements do not affect the intensity measurement, they are included to compensate the intensity losses in the fourth element. Denoting the intensity distribution recorded with a CCD camera after the element STn by $I_n(t)$, $n \in \{1, \ldots, 4\}$, the Stokes parameters are obtained as [36]

$$S_0(t) = I_1(t) + I_2(t), \tag{25a}$$

$$S_1(t) = I_1(t) - I_2(t), \tag{25b}$$

$$S_2(t) = 2I_3(t) - I_1(t) - I_2(t), \tag{25c}$$

$$S_3(t) = 2I_4(t) - I_1(t) - I_2(t), \tag{25d}$$

which are evaluated at each camera pixel.

4.1. Experimental results

First we assess the change in the Pancharatnam–Berry geometric phase when the polarization state of the frequency-shifted beam is rotated and the intensity ratio of the two beams is held at an arbitrarily chosen value $S_0'/S_0'' \approx 2.10$. We start with M5 removed and the beams having orthogonal (linear) polarization states corresponding to the HWP fast axis set to $\theta = 45°$ with respect to the x axis. The intensities S_0' and S_0'' are measured by blocking the beam in the other arm, followed by recording the temporal intensity modulation, $S_0(t)$, when both beams are allowed simultaneously to the detector. After the reduction of the background noise from the measured data, we subject the beating signal to a sine fitting procedure and extract $|\gamma_0|$ in accordance with equation (24). This is then used to calculate the geometric phase from equation (23) with $N = 200$. We repeat the measurements several times and obtain the average value $\phi_{PB} = 0.641\pi \pm 0.001\pi$, where the error is
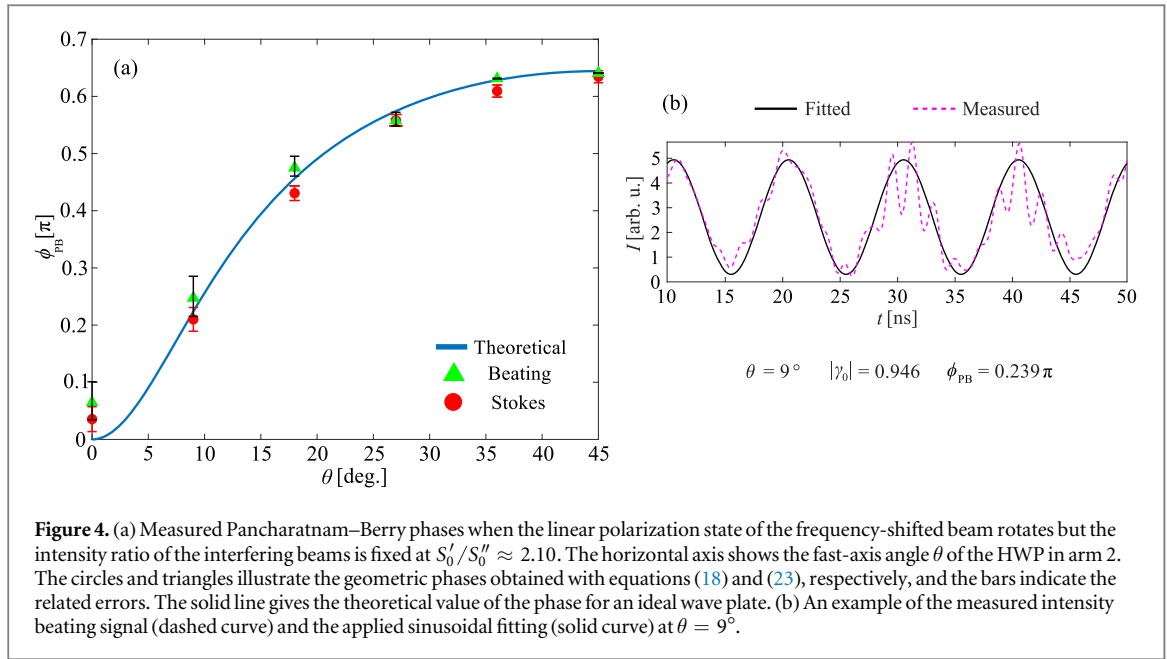
Figure 4. (a) Measured Pancharatnam–Berry phases when the linear polarization state of the frequency-shifted beam rotates but the intensity ratio of the interfering beams is fixed at $S_0'/S_0'' \approx 2.10$. The horizontal axis shows the fast-axis angle θ of the HWP in arm 2. The circles and triangles illustrate the geometric phases obtained with equations (18) and (23), respectively, and the bars indicate the related errors. The solid line gives the theoretical value of the phase for an ideal wave plate. (b) An example of the measured intensity beating signal (dashed curve) and the applied sinusoidal fitting (solid curve) at $\theta = 9°$.
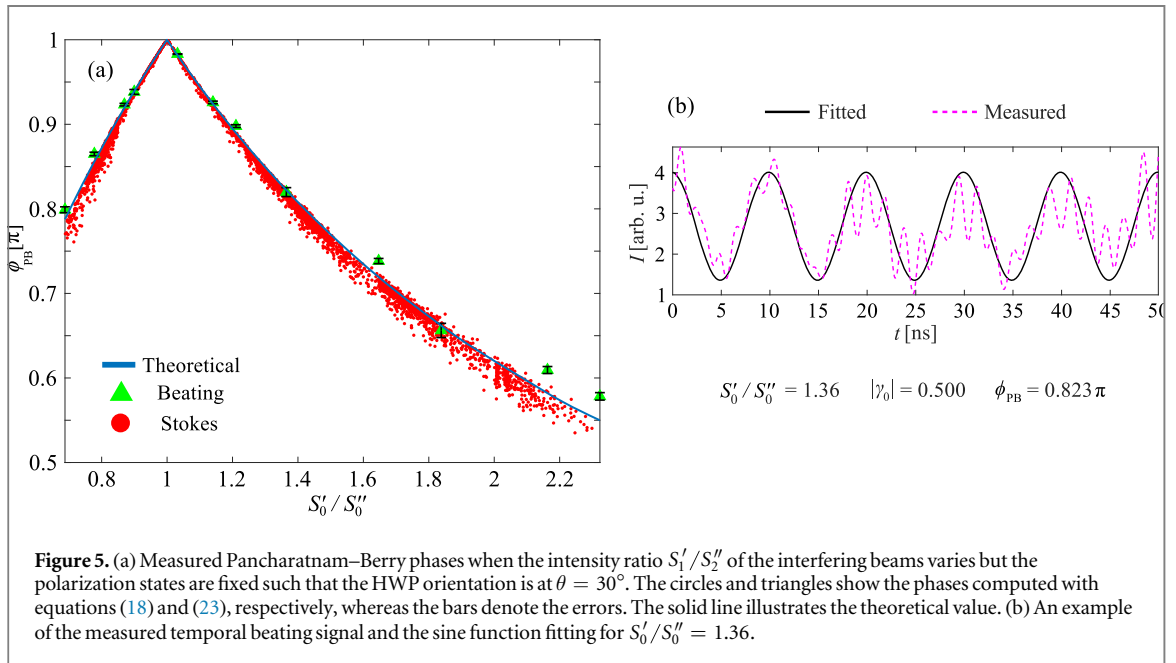

Figure 5. (a) Measured Pancharatnam–Berry phases when the intensity ratio S_1'/S_2'' of the interfering beams varies but the polarization states are fixed such that the HWP orientation is at $\theta = 30°$. The circles and triangles show the phases computed with equations (18) and (23), respectively, whereas the bars denote the errors. The solid line illustrates the theoretical value. (b) An example of the measured temporal beating signal and the sine function fitting for $S_0'/S_0'' = 1.36$.

estimated via standard deviation. Next we use the second measurement system, with mirror M5 in place, to measure the Stokes parameters for the individual beams. Using the CCD array camera, we record the spatial S_0' and S_0'' distributions as well as the Poincaré vectors $\mathbf{P}'$ and $\mathbf{P}''$ at pixels where $S_0'/S_0'' \approx 2.10$. The Pancharatnam–Berry phase is then obtained from equation (18). Averaging the phases over multiple points gives $\phi_{PB} = 0.634\pi \pm 0.011\pi$, where the error is again obtained from standard deviation.

The above procedure is applied to a case in which the linear polarization of the beam in arm 2 is tilted by rotating the HWP from $\theta = 45°$ (orthogonal polarizations) to $\theta \approx 0°$ (nearly parallel polarizations) in steps of $9°$. The related geometric phases obtained with equations (18) and (23) are shown in figure 4(a) with circles and triangles, respectively, along with a representative example of the intensity beating (dashed curve) and the sinusoidal fitting (solid curve) in figure 4(b). In the latter figure (and in figure 5(b)), the extra high-frequency variations originate from weak, fast intensity oscillations (520 MHz) of the laser diode we used. In figure 4(a) the solid curve gives the theoretical phase behavior when an ideal wave plate rotates the polarization. We immediately see that the two experimental methods are in good agreement with each other and with the theory, especially when the polarization states approach orthogonal situation. The differences are more noticeable when the polarization states are (nearly) parallel, a case where even a small change in $|\gamma_0|$ can significantly alter the

estimate for the geometric phase. As an example, setting $S_0'/S_0'' = 2.10$ and employing equation (23) with $|\gamma_0| = 0.98$ and $|\gamma_0| = 0.99$ implies $\phi_{\mathrm{PB}} = 0.114\pi$ and $\phi_{\mathrm{PB}} = 0.062\pi$, respectively.

In the second experiment, the polarization state of the beam in arm 2 is fixed with the HWP set at $\theta = 30°$ while the intensity ratio of the beams is changed with the ND filter in arm 1. We modify the ratio S_0'/S_0'' between 0.69 and 2.32 and measure the geometric phase in the two ways described above. The results are shown in figure 5(a) where again the circles and triangles correspond to the phases obtained with equations (18) and (23), respectively, and the solid curve depicts the theoretical value. Figure 5(b) represents an example of the measured beating signal (dashed curve) for the intensity ratio $S_0'/S_0'' = 1.36$ as well as the associated fitting (solid curve). Notice that for the various ND filter strengths, we considered the CCD pixels at which $0.69 < S_0'/S_0'' < 2.32$ and used these positions to compute the Pancharatnam–Berry phase. The set of dots in figure 5(a) refers to these pixel-wise phase values (for clarity only every tenth value was retained in the figure). We see that, in general, the two experimental methods are in good agreement with each other and with the theoretical prediction. Deviations from the theoretical value are observed to slightly increase with increasing intensity difference.

5. Conclusions

We studied theoretically and experimentally the Pancharatnam–Berry phase associated with the polarization beating produced by the interference of two monochromatic electromagnetic optical beams of different frequencies—a context where a geometric phase has not been considered before. The geometric phase originates from the periodicity of the polarization Stokes parameters whose normalized Poincaré vector was proven to traverse a closed circular trajectory on the Poincaré sphere during a single beating cycle. The related field variations were confirmed to satisfy Pancharatnam's connection over the path. The Pancharatnam–Berry phase, obtained as half the solid angle covered by the polarization loop on the Poincaré sphere, assumed a compact form in terms of the intensity and polarization information of the interfering beams. In addition, we demonstrated that the geometric phase can equally be evaluated from the intensities of the individual beams and the amplitude of the intensity beating. The validities of the two methods to extract the Pancharatnam–Berry phase were verified experimentally using an interferometer with a fast detector and a specific polarimetric setup. A key finding of our work was that while the total phase difference across a beating period depends only on the frequencies of the interfering beams, the geometric and dynamical phases comprising the phase difference both depend on their polarization states and the intensities. Thus, contributions of the geometric and dynamical phases can be adjusted by varying the intensities and polarization characteristics of the beams. A change in one phase leads to a change in the other indicating an entangled nature of the two, a feature characteristic to polarization beating. Our results offer new foundational insight into geometric phases and the role of polarization in temporal electromagnetic interference. In particular, our work reveals an extraordinary rich phase structure connected to a seemingly simple physical phenomenon of beating.

Acknowledgments

ORCID iDs

Matias Koivurova ⓘ https://orcid.org/0000-0001-6100-6316

References

[1] Saleh B E A and Teich M C 2007 *Fundamentals of Photonics* (Hoboken, NJ: Wiley)
[2] Milonni P W and Eberly J H 2010 *Laser Physics* (Hoboken, NJ: Wiley)
[3] Kingston R H 1995 *Optical Sources, Detectors, and Systems: Fundamentals and Applications* (Cambridge, MA: Academic)
[4] Greiner C, Boggs B, Wang T and Mossberg T W 1998 Laser frequency stabilization by means of optical self-heterodyne beat-frequency control *Opt. Lett.* **23** 1280–2
[5] Eichholz J, Tanner D B and Mueller G 2015 Heterodyne laser frequency stabilization for long baseline optical interferometry in space-based gravitational wave detectors *Phys. Rev.* D **92** 022004
[6] Coupland J M 2000 Laser doppler and pulsed laser velocimetry in fluid mechanics *Photomechanics* (*Topics in Applied Physics* Vol 77) ed P K Rastogi (Berlin: Springer) pp 373–412
[7] Razdan K and Van Baak D A 2002 Demonstrating optical beat notes through heterodyne experiments *Am. J. Phys.* **70** 1061–7
[8] McDonald M, Ha J, McGuyer B H and Zelevinsky T 2014 Visible optical beats at the hertz level *Am. J. Phys.* **82** 1003–5

[9] Lajunen H, Salaj J and Setälä T 2016 Polarization beating of random electromagnetic beams *J. Eur. Opt. Soc.-Rapid* **11** 16011

[10] Shevchenko A, Roussey M, Friberg A T and Setälä T 2017 Polarization time of unpolarized light *Optica* **4** 64–70

[11] Shapere A and Wilczek F 1989 *Geometric Phases in Physics* (Singapore: World Scientific)

[12] Anandan J 1992 The geometric phase *Nature* **360** 307–13

[13] Aravind P K 1992 A simple proof of Pancharatnam's theorem *Opt. Commun.* **94** 191–6

[14] Pancharatnam S 1956 Generalized theory of interference, and its applications *Proc. Ind. Acad. Sci.* A **44** 247–62

[15] Bhandari R 1997 Polarization of light and topological phases *Phys. Rep.* **281** 1–64

[16] Berry M V 1984 Quantal phase factors accompanying adiabatic changes *Proc. R. Soc.* A **392** 45–57

[17] Berry M V 1987 The adiabatic phase and Pancharatnam's phase for polarized light *J. Mod. Opt.* **34** 1401–7

[18] Berry M V 1990 Anticipations of the geometric phase *Phys. Today* **43** 34–40

[19] Tomita A and Chiao R Y 1986 Observation of Berry's topological phase by use of an optical fiber *Phys. Rev. Lett.* **57** 937–40

[20] Chyba T H, Wang L J, Mandel L and Simon R 1988 Measurement of the Pancharatnam phase for a light beam *Opt. Lett.* **13** 562–4

[21] Bhandari R and Samuel J 1988 Observation of topological phase by use of laser interferometer *Phys. Rev. Lett.* **60** 1211–3

[22] Simon R, Kimble H J and Sudarshan E C G 1988 Evolving geometric phase and its dynamical manifestation as a frequency shift: an optical experiment *Phys. Rev. Lett.* **61** 19–22

[23] Kwiat P G and Chiao R Y 1991 Observation of nonclassical Berry's phase for the photon *Phys. Rev. Lett.* **66** 588–91

[24] Hariharan P 2006 The geometric phase *Progress in Optics* vol 48 ed E Wolf (Amsterdam: Elsevier) pp 149–201

[25] Daniel S, Saastamoinen K, Saastamoinen T, Vartiainen I, Friberg A T and Visser T D 2017 Surface plasmons carry the Pancharatnam–Berry geometric phase *Phys. Rev. Lett.* **119** 253901

[26] Hannonen A, Partanen H, Tervo J, Setälä T and Friberg A T 2019 Pancharatnam–Berry phase in electromagnetic double-pinhole interference *Phys. Rev.* A **99** 053826

[27] Balthasar Mueller J P, Rubin N A, Devlin R C, Groever B and Capasso F 2017 Metasurface polarization optics: independent phase control of arbitrary orthogonal states of polarization *Phys. Rev. Lett.* **118** 113901

[28] Maguid E, Yulevich I, Yannai M, Kleiner V, Brongersma M L and Hasman E 2017 Multifunctional interleaved geometric-phase dielectric metasurfaces *Light Sci. Appl.* **6** e17027

[29] Minovich A E and Zayats A V 2018 Geometric-phase metasurfaces based on anisotropic reflection: generalized design rules *ACS Photonics* **5** 1755–61

[30] Brosseau C 1998 *Fundamentals of Polarized Light: A Statistical Optics Approach* (Hoboken, NJ: Wiley)

[31] Gil J J and Ossikovski R 2016 *Polarized Light and the Mueller Matrix Approach* (Boca Raton, FL: CRC Press)

[32] Korotkova O and Wolf E 2005 Generalized Stokes parameters of random electromagnetic beams *Opt. Lett.* **30** 198–200

[33] Tervo J, Setälä T, Roueff A, Réfrégier P and Friberg A T 2009 Two-point Stokes parameters: interpretation and properties *Opt. Lett.* **34** 3074–6

[34] Setälä T, Tervo J and Friberg A T 2006 Stokes parameters and polarization contrasts in Young's interference experiment *Opt. Lett.* **31** 2208–10

[35] Leppänen L-P, Saastamoinen K, Friberg A T and Setälä T 2014 Interferometric interpretation for the degree of polarization of classical optical beams *New J. Phys.* **16** 113059

[36] Goldstein D 2003 *Polarized Light* 2nd edn (Boca Raton, FL: CRC Press)